Electrical and magnetic studies of (Cu/Zn)-bonded $Sm_2Fe_{17}M_xN_y$ magnets (M=B or C)

Y. D. Yao
Institute of Physics, Academia Sinica, Taipei 115, Taiwan, Republic of China and Department of Physics, National Chung Cheng University, Chia-yi 621, Taiwan, Republic of China

P. C. Kuo
Institute of Materials Engineering, National Taiwan University, Taipei 107, Taiwan, Republic of China

W. C. Chang
Department of Physics, National Chung Cheng University, Chia-yi 621, Taiwan, Republic of China

C. J. Liu
Institute of Materials Engineering, National Taiwan University, Taipei 107, Taiwan, Republic of China

Samples of (Cu/Zn)-bonded and unbonded $Sm_2Fe_{17}M_xN_y$ with M=B or C ($x=0$, 0.25, and 0.5; $y<3$) were fabricated. All the samples, besides those with B, show single Curie temperature T_C and with Sm_2Fe_{17}-type crystal structure; however, multiphase structure and double T_C were observed in all the samples with B. For all the heating runs the electrical resistivity roughly above 600 K increases abruptly for all Zn-bonded samples; and decreases abruptly for all Cu-bonded samples. After these high temperature runs, the residual electrical resistivity increases for all Zn-bonded samples, and decreases for all Cu-bonded samples. The effects of Cu segregation and Zn reaction with samples are identified by the EPMA analyses.

Interstitial nitrides $Sm_2Fe_{17}N_y$ magnets discovered by Coey *et al.*[1] have been extensively studied during the past few years, e.g., Refs. 1–9. It was found that the effect of nitrogen on the structure is to expand the unit cell without changing the symmetry of the 2:17 parent compound. $Sm_2Fe_{17}N_y$ compound possesses high Curie temperature, a strong uniaxial anisotropy field, and a high saturation magnetization, which are comparable or superior to those of $Nd_2Fe_{14}B$. However, $Sm_2Fe_{17}N_y$ is metastable and decomposes to SmN and α-Fe at high temperatures roughly above 650 °C.[10] In general, low-temperature-melting metals such as Zn, Sn, and In or organic resins such as epoxy are used to form $Sm_2Fe_{17}N_y$ bonded magnets.[11–15]

Samples for this study were prepared from commercially available high purity Sm(99.9%), Fe(99.99%), C, B, and nitrogen gas. The Sm_2Fe_{17} ingots were prepared by arc melting technique, followed by an anneal in vacuum at 1270 K for two days. For samples containing C or B, the C and B were added during the arc-melting process. These ingots were crushed and milled to powders with the average particle size of 10 μm. The temperature for nitrogenation is in the range from 700 to 800 K. In order to avoid a possible phase transition during cooling the quartz tubes were water quenched afterwards. For bonded samples, the milled samples were blended with 25 wt % of Zn or Cu powders (−325 mesh), and pressed into pellets with a pressure of 4 tons/cm^2 in a magnetic field of 1 T. Pellets were then heat treated in N_2 for 2 h at temperatures of 620–720 K for Zn-bonded samples, and of 620–800 K for Cu-bonded samples. All the samples were characterized by powder x-ray diffraction, scanning electron microscopy (SEM) with electron probe microanalysis (EPMA) and differential scanning calorimeter (DSC), etc.

The electrical resistivity and magnetization of these samples were measured as functions of temperatures between 4 and 1200 K. For the magnetization studies, both vibration sample magnetometer (VSM) and superconducting quantum interference device (SQUID) were used to determine the magnetization.

Powder x-ray diffraction analyses show that the Sm_2Fe_{17} phase with the Th_2Zn_{17} crystal structure exists in our samples; however, a small amount of α-Fe is always presented in most of our samples. Multiphase structure was observed in the samples with B. As an example, the powder x-ray diffraction patterns observed for Sm_2Fe_{17}, $Sm_2Fe_{17}C_{0.5}$, $Sm_2Fe_{17}B_{0.5}$, and $Sm_2Fe_{17}N_{2.6}$ samples are shown in Fig. 1 (a) to 1 (d), respectively. It is clearly that the 2 : 17 phase peaks in (b) and (d) are shifted to lower angles in comparison with (a) for Sm_2Fe_{17}; their lattice parameters a and b were roughly calculated from the powder x-ray diffraction pattern to be $a=8.58$, 8.63, 8.71 Å, and $b=12.41$, 12.45, 12.61 Å, for Sm_2Fe_{17}, $Sm_2Fe_{17}C_{0.5}$, and $Sm_2Fe_{17}N_y$, respectively. Curve (b) in Fig. 1 shows multiphase structure in $Sm_2Fe_{17}B_{0.5}$.

The temperature dependence of the magnetization M at 8 kG of the samples had been studied between 4 and 1100 K. The value of the magnetization at 4 K are roughly between 100 and 120 emu/g for all the unbounded samples, and between 80 and 100 emu/g for all (Zn/Cu)-bonded samples. Typically, four kinds of behaviors have been observed; as an example, Fig. 2 presents the normalized magnetization M/M_0 as functions of temperature for (a) Sm_2Fe_{17}, (b) $Sm_2Fe_{17}C_{0.5}$, (c) $Sm_2Fe_{17}B_{0.5}$, and (d) $Sm_2Fe_{17}N_{2.6}$. M_0 is the magnetization at 4 K and 8 kG for each sample. Clearly, the magnetization roughly above 900 K increase slowly and then drop abruptly around 1040 K with increasing temperature. This suggests that α-Fe is precipitated roughly above 900 K. Besides the Curie temperature T_c of α-Fe around 1040 K, the curves show single T_c around 390 K for Sm_2Fe_{17}, around 540 K for $Sm_2Fe_{17}C_{0.5}$, and around 780 K for $Sm_2Fe_{17}N_{2.6}$. However, double T_c around 400 and 600 K had

 0021-8979/94/75(10)/6244/3/$6.00

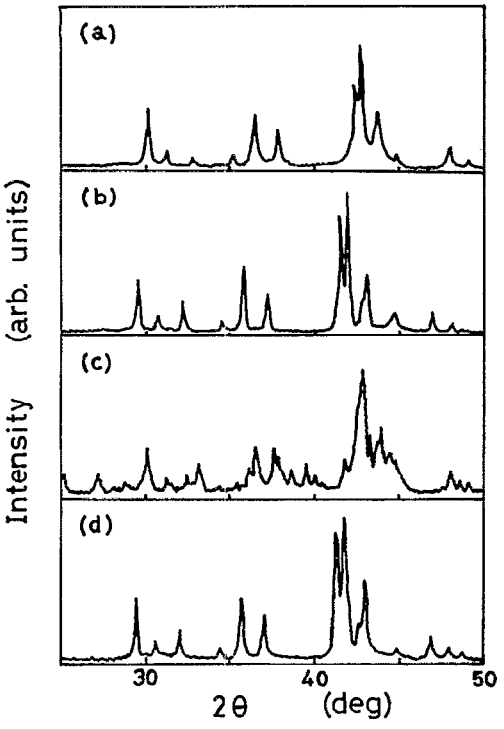

FIG. 1. The powder x-ray diffraction patterns for (a) Sm_2Fe_{17}, (b) $Sm_2Fe_{17}C_{0.5}$, (c) $Sm_2Fe_{17}B_{0.5}$, and (d) $Sm_2Fe_{17}N_{2.6}$ samples.

observed for all the $Sm_2Fe_{17}B_x$ samples. From the x-ray diffraction pattern, the electrical resistivity, and the magnetization studies, we conclude that besides the α-Fe phase, at least two major mixture phases with T_c around 400 and 600 K, are coexisted in the $Sm_2Fe_{17}B_x$ magnets. We guess that they may be the Sm_2Fe_{17} and $Sm_2Fe_{14}B$ phases.

The electrical resistivity ρ of the bulk $Sm_2Fe_{17}M_x$ (M=C or B; x=0, 0.25, and 0.5) samples has been studied with increasing and decreasing temperatures between 4 and 1200 K. Each resistivity curve approaches to a constant residual resistivity near 4 K; and its value decreases after the high temperature run. This indicates that the scattering centers for the conduction electrons are decreased after high temperature runs; and also suggests that α-Fe and other ordered phases

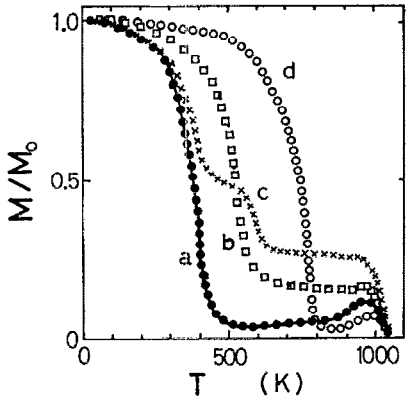

FIG. 2. The normalized magnetization as a function of temperature for (a) Sm_2Fe_{17}, (b) $Sm_2Fe_{17}C_{0.5}$, (c) $Sm_2Fe_{17}B_{0.5}$, and (d) $Sm_2Fe_{17}N_{2.6}$ samples.

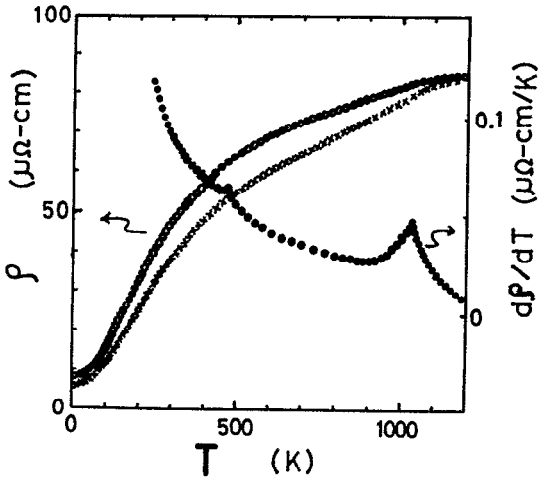

FIG. 3. The electrical resistivity and its derivative $d\rho/dT$ of the $Sm_2Fe_{17}C_{0.25}$ sample as functions of T between 4 and 1200 K. (○: heating run, ×: cooling run, and ●: $d\rho$/dT for heating run.)

may be precipitated after the high temperature runs. Typically, Fig. 3 presents the electrical resistivity data of $Sm_2Fe_{17}C_{0.25}$ sample. The open circle and cross are associated with heating and cooling runs, respectively. The derivative of the electrical resistivity with respect to temperature for the heating run is plotted by dots in Fig. 3. T_c determined from the peak of $d\rho/dT$ are 480 K for $Sm_2Fe_{17}C_{0.25}$ phase and 1040 K for α-Fe phase.

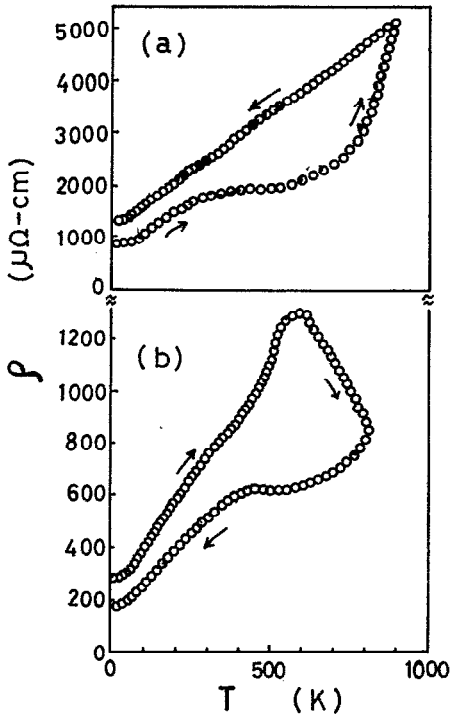

FIG. 4. The electrical resistivity as a function of T between 4 and 1000 K for (a) Zn-bonded $Sm_2Fe_{17}N_{2.0}$, and (b) Cu-bonded $Sm_2Fe_{17}C_{0.25}N_{2.6}$ (The sequence of the heating and cooling runs is indicated by arrows.)

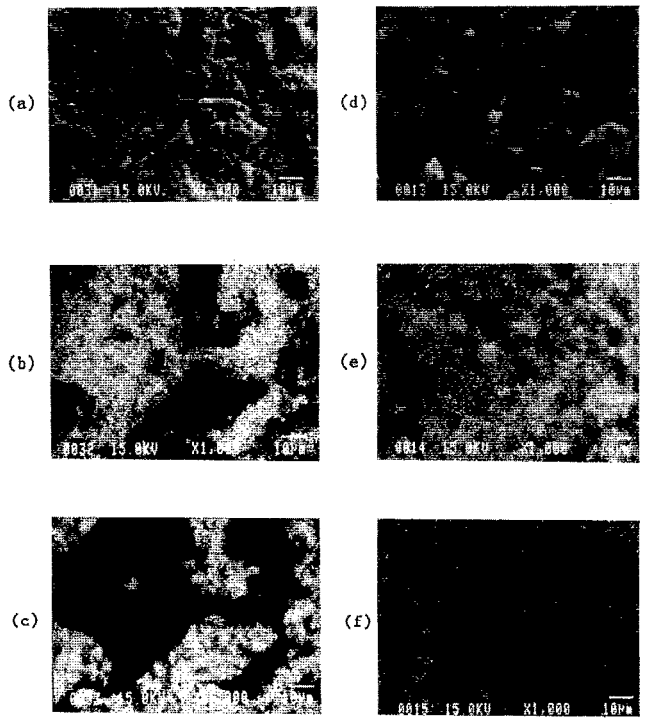

FIG. 5. (a) The SEM micrograph of the Cu-bonded $Sm_2Fe_{17}C_{0.25}N_{2.6}$ after the high temperature resistivity measurement. (b) The EPMA picture of (a) for Fe-rich distribution. (c) The EPMA picture of (a) for Cu-rich distribution. (d) The SEM micrograph of the Zn-bonded $Sm_2Fe_{17}N_{2.0}$ after the high temperature resistivity measurement. (e) The EPMA picture of (d) for Fe-rich distribution. (f) The EPMA picture of (d) for Zn-rich distribution.

The coercivity H_c of the Zn-bonded samples can be improved to 6–14 kOe after annealing them between 620 and 720 K in N_2 for 2 h. However, H_c of the Cu-bonded samples was only reached 1–3 kOe after annealing them between 620 and 800 K in N_2 for 2 h. Generally speaking, from the DSC investigations below 700 K for all the (Zn/Cu)-bonded samples, we found that an exotherm peak between 600 and 700 K for all the bonded samples, and an endothermic peak between 400 and 450 K for Cu-bonded samples only. The exotherm peak has been explained to be the onset temperature of the nitrogen absorption into Sm_2Fe_{17}.[16] It is not clear at present about the corresponding changes correlated to the exdothermic peak for all the Cu-bonded samples. However, it seems to relate the slope increase of the resistivity near 450 K with increasing temperature for all the Cu-bonded samples as shown in Fig. 4.

In general, the temperature dependence of the magnetization at 8 kG for all the (Zn/Cu)-bonded $Sm_2Fe_{17}M_xN_y$ samples behaves quite similarly to the curve d in Fig. 2 with T_c around 780 K. However, this two bonded groups show completely different behaviors for the temperature dependence of ρ with increasing and decreasing temperatures between 4 and 1000 K. The typical behaviors are that (1) for all Zn-bonded samples, the heating run ρ increases abruptly roughly above 600 K, and the value of ρ for the cooling run is always higher than that of heating run; (2) for all Cu-bonded samples, the heating run ρ decreases abruptly roughly above 600 K, and the value of cooling run ρ is always lower than that of the heating run. In Fig. 4, as an example, curve a shows the ρ of Zn-bonded $Sm_2Fe_{17}N_{2.0}$ samples, and curve b shows the ρ of Cu-bonded $Sm_2Fe_{17}C_{0.25}N_{2.6}$ samples. The sequence of the heating and cooling runs is indicated by arrows in the figures.

From the EPMA investigations of the SEM micrographs of the (Zn/Cu)-bonded samples, we found that in the Cu-bonded samples after the high temperature measurements the Fe-rich and Cu-rich areas are completely distinguishable. As shown in Fig. 5, (a) is the SEM micrograph of the Cu-bonded $Sm_2Fe_{17}C_{0.25}N_{2.6}$ sample after the electrical resistivity measurements; (b) is the EPMA picture of Fig. 5(a) for the Fe-rich distribution (white regions); and (c) is the EPMA picture of Fig. 5(a) for the Cu-rich distribution (white regions). However, it is difficult to separate the Fe-rich and Zn-rich regions in Zn-bonded samples. As an example, Fig. 5(d) is the SEM micrograph of the Zn-bonded $Sm_2Fe_{17}N_{2.0}$ sample after the electrical resistivity measurements; (e) is the EPMA picture of Fig. 5(d) for the Fe-rich distribution (white regions); and (f) is the EPMA picture of Fig. 5(d) for the Zn-rich distribution (white regions).

Finally, for Cu-bonded samples, the main reason for the decrease of ρ after high temperature runs is due to the segregation of Cu and precipitation of Fe, so that the scattering center for conducting electrons is reduced; however, the variation of the magnetization and coercivity is small after the Cu bonding. For Zn-bonded samples, the main reason for the increase of ρ after high temperature runs is due to the chemical reactions between Zn and $Sm_2Fe_{17}M_xN_y$; and under proper annealing, the variation of magnetization is small, but the coercivity can be enhanced up to 14 kOe.

This work was supported by the National Science Council of the ROC through Grant No. NSC82-0212-M-194-016.

[1] J. M. D. Coey and H. Sun, J. Magn. Magn. Mater. **87**, L251 (1990).
[2] M. Katter, J. Wecker, L. Schultz, and R. Grossinger, J. Magn. Magn. Mater. **92**, L14 (1990).
[3] A. Fukuno, C. Ishizaka, and T. Yoneyama, J. Appl. Phys. **70**, 6021 (1991).
[4] J. Ding, P. G. McCormick, and R. Street, Appl. Phys. Lett. **61**, 2721 (1992).
[5] J. P. Woods, A. S. Fernando, S. S. Jaswal, B. M. Patterson, D. Welipitiya, and D. J. Sellmyer, J. Appl. Phys. **73**, 6913 (1993).
[6] K. I. Machida, Y. Nakatani, A. Onodera, and G. Y. Adachi, Jpn. J. Appl. Phys. **32**, L837 (1993).
[7] R. Skomski and J. M. D. Coey, J. Appl. Phys. **73**, 7602 (1993).
[8] G. J. Long, O. A. Pringle, F. Grandjean, W. B. Yelon, and K. H. J. Buschow, J. Appl. Phys. **74**, 504 (1993).
[9] R. Skomski, K.-H. Müller, P. A. P. Wendhausen, and J. M. D. Coey, J. Appl. Phys. **73**, 6047 (1993).
[10] Y. Otani, D. P. F. Hurley, H. Sun, and J. M. D. Coey, J. Appl. Phys. **69**, 5584 (1991).
[11] M. Q. Huang, L. Y. Zhang, B. M. Ma, Y. Zheng, J. M. Elbicki, W. E. Wallace, and S. G. Sankar, J. Appl. Phys. **70**, 6027 (1991).
[12] Y. Otani, A. Monkarika, H. Sun, J. M. D. Coey, E. Devlin, and I. R. Harris, J. Appl. Phys. **69**, 6735 (1991).
[13] P. A. P. Wendhausen, A. Handstein, P. Nothnagel, D. Eckert, and K.-H. Müller, Phys. Status Solidi A **127**, K121 (1991).
[14] W. Rodewald, B. Wall, M. Katter, M. Velicescu, and P. Schrey, J. Appl. Phys. **73**, 5899 (1993).
[15] P. A. P. Wendhausen, D. Eckert, A. Handstein, K.-H. Müller, G. Leitner, and R. Skomski, J. Appl. Phys. **73**, 6044 (1993).
[16] X. C. Kou, R. Grössinger, M. Katter, J. Wecker, L. Schultz, T. H. Jacobs, and K. H. J. Buschow, J. Appl. Phys. **70**, 2272 (1991).